This article has been accepted for inclusion in a future issue of this journal. Content is final as presented, with the exception of pagination.

The Influence of Spectral Albedo on Bifacial Solar Cells: A Theoretical and Experimental Study

Thomas C. R. Russell, Rebecca Saive, André Augusto, Stuart G. Bowden, and Harry A. Atwater

***Abstract*—We have investigated the influence of the spectral albedo on the power output of bifacial solar cells. We adapted the Shockley–Queisser radiative flux balance framework to account for a variation of the spectrum and intensity of the incoming light. We find that the ideal band gap and the maximum efficiency depend on the spectral albedo of the surroundings and that optimal cell performance cannot be assessed when only accounting for a spectrally independent albedo. With a spectral albedo model, we predict that the power output for a bifacial silicon solar cell surrounded by green grass is 3.1% higher than for a wavelength-independent albedo, and even 5.2% higher for white sand. We experimentally verify this trend for silicon heterojunction solar cells and we derive the ideal spectral albedo.**

***Index Terms*—Bifacial solar cells, Shockley–Queisser limit, spectral albedo, thermodynamic efficiency limit.**

I. Introduction

INCREASING the power output of solar modules is a crucial step toward lowering the cost of electricity generated by photovoltaic power plants [1], [2]. One strategy for increased power output is the use of bifacial solar cells that are designed to accept incident light at the front and rear of the cells. This concept was already developed in the 1960s [3], but only recently module manufacturers started selling bifacial modules as a standard technology. The gain from using a bifacial configuration often exceeds the power output of monofacial solar modules by a surprising amount, and values of up to 50% have been reported [4]. A more recent study shows that the bifacial power gain ranges between 13% and 35% under sunny condition and 40% and 70% under cloudy conditions, depending on the height of the ground clearance [5]. However, it is difficult to predict the power output of a bifacial solar cell as it strongly depends on the albedo of the surroundings as well as on the geometry in which the cells are mounted [6]. The geometric factors are the tilt, the height above ground, and length of the solar module. These geometric factors affecting the bifacial solar cell efficiency have been extensively studied elsewhere [6]–[13], and here we address the influence of the albedo. The albedo is a measure for how well a surface reflects light and it is defined as the ratio between the power of the reflected light and the power of the total incoming light. The albedo depends strongly on the surface properties. As examples, green grass exhibits an albedo of 0.24 and white sand shows an albedo of 0.67. Accepting this additional photon flux of light reflected from the ground leads to effective light concentration within the cell. Therefore, both the voltages and currents of the cells increase. However, the albedo of typical reflective surfaces also exhibits a spectral dependence—which is evident from the examples of green grass and white sand—that affects solar cell performance [14], [15]. An overview of the spectral and effective albedo of several ubiquitous surfaces is shown in Fig. 1. Taking this spectral dependence into account can lead to deviations from the optimal thermodynamic operating point and the maximum achievable power efficiency as we report here.

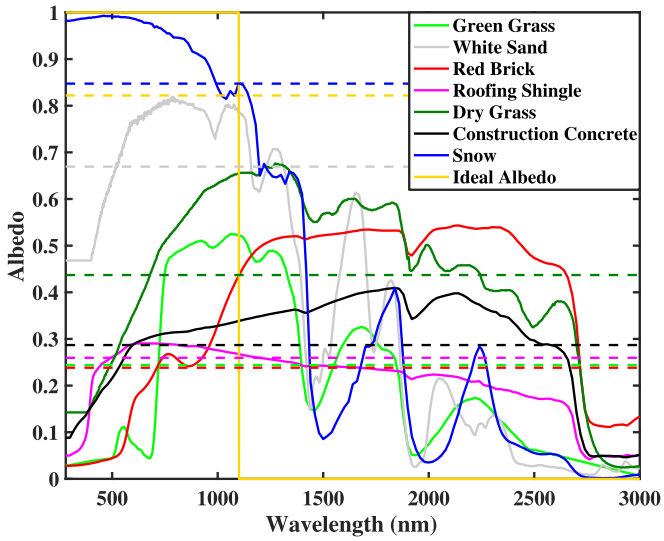

Fig. 1. Spectral and effective (dashed lines) albedo of several widely used surfaces. The ideal albedo for silicon photovoltaic modules is shown in yellow.

First, we present an investigation of the thermodynamic efficiency limit for bifacial solar cells with and without taking the spectral dependence of the albedo into account. We apply the model of Shockley and Queisser [16] to this case and calculate

Manuscript received May 16, 2017; revised July 25, 2017 and August 24, 2017; accepted September 15, 2017. This work was supported in part by the Engineering Research Center Program of the National Science Foundation and the Office of Energy Efficiency and Renewable Energy of the Department of Energy under NSF Cooperative Agreement No. EEC-1041895 and in part by the U.S. Department of Energy through the Bay Area Photovoltaic Consortium under Award Number DE-EE0004946. The work of R. Saive was supported by the Global Climate & Energy project. *(Thomas C. R. Russell and Rebecca Saive contributed equally to this work.) (Corresponding author: Rebecca Saive.)*

T. C. R. Russell, R. Saive, and H. A. Atwater are with the Thomas J. Watson Laboratories of Applied Physics and Material Science, California Institute of Technology, Pasadena, CA 91125 USA (e-mail: thomruss@caltech.edu; rebsaive@caltech.edu; haa@caltech.edu).

A. Augusto and S. G. Bowden are with the Department of Electrical Engineering, Arizona State University, Tempe, AZ 85287-5706 USA (e-mail: augusto@asu.edu; sgbowden@asu.edu).

Color versions of one or more of the figures in this paper are available online at http://ieeexplore.ieee.org.

Digital Object Identifier 10.1109/JPHOTOV.2017.2756068

2156-3381 © 2017 IEEE. Translations and content mining are permitted for academic research only. Personal use is also permitted, but republication/redistribution requires IEEE permission. See http://www.ieee.org/publications_standards/publications/rights/index.html for more information.

This article has been accepted for inclusion in a future issue of this journal. Content is final as presented, with the exception of pagination.

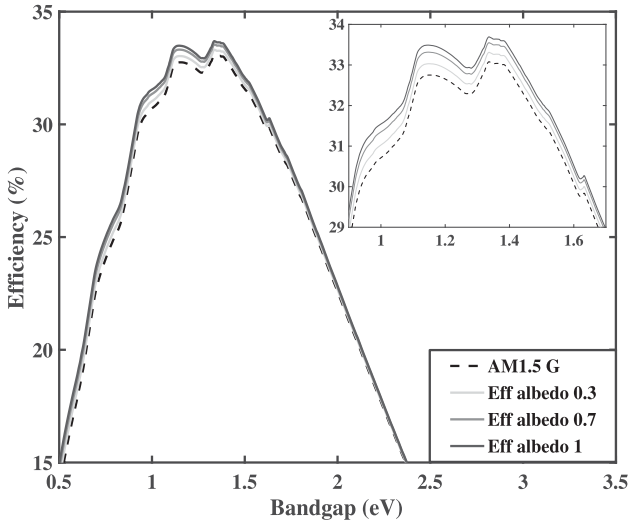

Fig. 2. Maximum conversion efficiency of bifacial solar cells for different effective albedos.

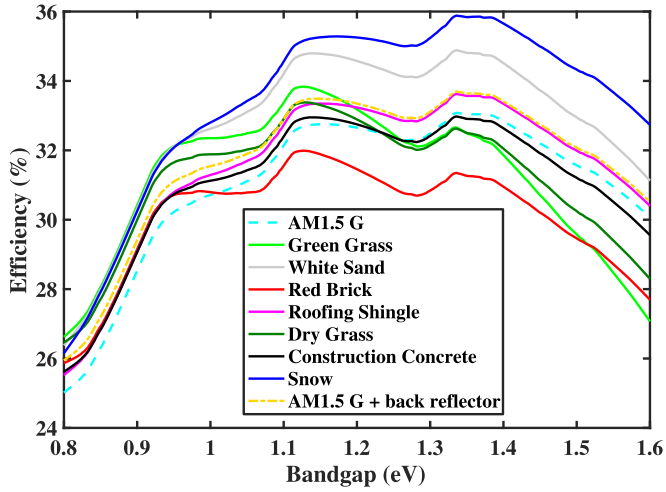

Fig. 3. Thermodynamic efficiency limit for different spectral albedos.

the maximum efficiency for bifacial solar cells surrounded by different materials.

We find that the maximum thermodynamic efficiency and power output increase for several realistic environmental conditions and decrease for others. In the case of green grass, the power output increases by 3.1% and for white sand by 5.2% due to a high flux of reflected photons with energy above band gap. We use these results to study the implications for silicon solar cells. More than 90% of the modules currently produced use silicon as the absorber material [17]. To date, the only bifacial modules available on the market use silicon cells, with different cell technologies [18]. We show experimentally that the maximum efficiency and maximum power output of silicon solar cells depend significantly on the spectral features of the albedo, and we derive the ideal spectral and effective albedo for silicon modules (see Fig. 1).

II. Thermodynamic Efficiency Limit With Spectral Independent Albedo

In order to calculate the power conversion efficiency, the Shockley–Queisser radiative flux balance [16], [19] was adapted to account for power gain due to the acceptance of reflected photons. The incoming optical flux consists of the sum of the front side AM 1.5G illumination (ASTM G-173-03) and ground-reflected rear illumination. At first, the albedo of the ground is assumed to be uniform and spectral independent, i.e., the ground has an effective albedo (R_A) [20]. Step-function absorption, with no absorption for photons with energy below bandgap, 100% absorption for photons with energy above band gap, is assumed here. The number of photons above bandgap ($m^{-2}{\cdot}s^{-1}$), accounting for an effective albedo, is enhanced by a factor $1 + R_A$ and thereby increasing the short-circuit current density. The open-circuit voltage (V_{OC}) is given by

$$V_{\mathrm{OC}} = \frac{k_B T_{\mathrm{Cell}}}{q} \ln\left(\frac{(1+R_A)\cdot I_S}{I_0} + 1\right) \tag{1}$$

in which I_S is the sunlight generated current, I_0 is the dark saturation current, and k_B is the Boltzmann constant. I_0 is affected by both radiative and nonradiative recombination processes. The radiative part of the dark current contains an extra factor of two in comparison with a monofacial cell since the bifacial solar cell has no back reflector, leading to a slight decrease in V_{OC}. The modeling is done for a solar cell temperature (T_{Cell}) of 300 K since it is close to the standard test conditions at which solar cells are measured [21]. The conversion efficiency of the bifacial cell increases with R_A, due to a logarithmic increase in V_{OC} (1). Fig. 2 shows the power conversion efficiency of a bifacial solar cell as a function of the bandgap energy for different values of R_A. A single-junction bifacial solar cell is considered. The maximum conversion efficiency can be obtained via

$$\eta_{\mathrm{Max}} = \frac{V_{\mathrm{OC}}\ J_{\mathrm{SC}}\ \cdot\ \mathrm{FF}\ \cdot\ (1+R_A)}{P_{\mathrm{SUN}}\ \cdot (1+R_A)} \tag{2}$$

in which FF is the fill factor, J_{SC} is the short-circuit current density, V_{OC} is the open-circuit voltage, and P_{SUN} is the solar constant of approximately 1000 W/m^2 total solar irradiance. The dashed black line represents the Shockley–Queisser limit for AM 1.5G spectrum, with no rear-side illumination and without back reflector. The Shockley–Queisser limit for the AM 1.5G spectrum assuming single junction, bandgap of 1.34 eV, and no back reflector is around 33.1% $(R_A = 0)$. The solar constant in the denominator of the equation for the power conversion efficiency (2) increases with R_A, i.e., the total incoming power is increased due to the ability of the back surface to intercept the scattered light. For increasing values of R_A between 0 and 1, the Shockley–Queisser limit is enhanced to a maximum of 33.7% for R_A equal to 1 and bandgap equal to 1.34 eV. The single junction monofacial solar cell with back reflector has a maximum efficiency of 33.7% for an optimal bandgap of 1.34 eV, due to a decrease in entropy loss of the free energy of incoming photons. So, either including a back reflector or assuming an effective albedo of 1 enhances V_{OC} and thereby the efficiency to 33.7% (see Fig. 2). The efficiency is the same, but the power output of the bifacial solar cell with an effective

This article has been accepted for inclusion in a future issue of this journal. Content is final as presented, with the exception of pagination.

albedo of 1 is doubled with respect to the monofacial panel with back reflector.

III. Thermodynamic Efficiency Limit With Spectral Albedo

To simulate spectral effects on the conversion efficiencies for bifacial solar cells, a wavelength-dependent albedo is introduced, i.e., spectral albedo. Data on spectral albedo were obtained from The ASTER spectral library version 2.0 of Jet Propulsion Laboratory [22].

We chose to investigate seven common surfaces both natural and artificial, including green grass, white sand, red brick, roofing shingle, dry grass, construction concrete, and snow. By considering a spectral albedo instead of an effective albedo, the incoming light spectrum on the rear side of the cell is no longer a constant fraction of the AM 1.5G spectrum but unique for each surface (see Fig. 1). The dashed lines in Fig. 1 show the effective albedos of the respective surfaces and are obtained via

$$R_A = \frac{\int_0^\infty R_A\,(E)\ \cdot\ \mathrm{AM\ 1.5G}\,(E)\ dE}{\int_0^\infty \mathrm{AM\ 1.5G}\,(E)\ dE}. \tag{3}$$

Both the short-circuit current density and open-circuit voltage need to be adapted to account for spectral albedos. J_{SC} and V_{OC} as a function of the bandgap for a certain spectral albedo $(R_A(E))$ are obtained, respectively, as

$$J_{\mathrm{SC,alb}} = q \cdot \int_{E_{\mathrm{gap}}}^{\infty} (1 + R_A\,(E)) \cdot \mathrm{AM\ 1.5G}\,(E) \cdot \frac{1}{E} dE \tag{4}$$

$$V_{\mathrm{OC,alb}} = \frac{k_B T_{\mathrm{Cell}}}{q} \ln\left(\frac{q \cdot \int_{E_{\mathrm{gap}}}^{\infty} (1+R_A\,(E)) \cdot \mathrm{AM\ 1.5G}\,(E) \cdot \frac{1}{E} dE}{I_0} + 1\right) \tag{5}$$

in which q is the electron charge, $R_A(E)$ is the albedo dependent on the photon energy, and AM 1.5G is the incoming solar spectrum. Furthermore, to obtain the spectral albedo-dependent power conversion efficiency, (2) has been adapted to the form

$$\eta_{\mathrm{Max,alb}} = \frac{V_{\mathrm{OC,alb}}\ \cdot J_{\mathrm{SC,alb}} \times \mathrm{FF}}{P_{\mathrm{SUN}}\ \cdot\ (1 + R_A)}. \tag{6}$$

Fig. 3 shows the power conversion efficiency for the different surfaces as a function of the bandgap energy with spectral albedo taken into account. For snow and white sand, the efficiency is higher than for cells with and without a mirror back reflector under AM 1.5G, and therefore exceeds the calculated efficiency with spectral independent albedo for all bandgaps. However, red brick yields an efficiency lower than the AM 1.5G case, and therefore performs worse than expected from the spectrally independent albedo. The maximum power conversion efficiency and optimal bandgap for a single-junction bifacial cell vary with the type of surface. With an optimal bandgap of 1.34 eV and maximum efficiency of 35.88%, using snow as reflective surface shows the largest enhancement in power conversion efficiency in comparison with the AM 1.5G spectrum. In the case of green grass, the optimal bandgap for power conversion is 1.13 eV which is closer to the bandgap of crystalline silicon. Table I presents an overview of the simulation results. The power output increases in each case with the additional photon flux generated through reflection from the surroundings. In the case of snow, the power output is increased by 7.5% when taking a spectrally dependent albedo into account and for white sand by 4.0%. However, for red brick, the power output is 2.9% lower than predicted when only taking the effective albedo into account. The power output for snow, when considering a spectral albedo, is even more than double the power output under AM 1.5G illumination for a cell without back reflector, even though the effective albedo of snow is less than one. A comparison with the spectral albedos presented in Fig. 1 shows that surfaces perform best when a large portion of the reflected light spectrum has energy above the semiconductor bandgap.

IV. Practical Implications for Bifacial Silicon Solar Cells

We calculated the maximum power conversion efficiency and power output for a 180 μm thick heterojunction with intrinsic thin layer (HIT) solar cell with the same spectrally reflecting surfaces as mentioned in Section III. The absorber material is crystalline silicon at 300 K with a bandgap of 1.125 eV [23]. The top and bottom of the cell consist of a 70 nm thick layer of indium tin oxide (ITO), 5 nm thick layer of p/n-type amorphous silicon, and a 5 nm thick layer of intrinsic silicon [24]. Both sides are assumed to be textured with optimal 1 μm high pyramids [25]. It has been shown elsewhere [26] that all additional losses to the open-circuit voltage that are not included in the original study of Shockley and Queisser can be accounted for via the following expression:

$$qV_{\mathrm{OC}} = qV_{\mathrm{OC-Ideal}} - kT\,|\ln(\eta_{\mathrm{ext}})| \tag{7}$$

in which $V_{\mathrm{OC-Ideal}}$ is the open-circuit voltage when only considering radiative recombination losses. V_{OC} in (7) is the by poor external luminescence efficiency penalized open-circuit voltage. It is assumed that the bifacial solar cell has an external luminescence efficiency η_{ext} of the state-of-the-art Sunpower silicon device of 0.57% [27]. Furthermore, a ray-tracing simulation was performed to calculate the absorption of the crystalline silicon, using LightTools software, and the optical properties of the surface were obtained from OPAL 2 [28]. The IQE is assumed to be one over the whole solar spectrum, and in that case, the absorption of the crystalline silicon is equal to the external quantum efficiency (EQE) of the silicon bifacial solar cell. Metallic front and back contacts were neglected in order to demonstrate the ideal case that can be realized by using effectively transparent contacts [29]–[31]. The EQE was used to calculate the short-circuit current density for various incoming photon fluxes, depending on the spectrally reflecting ground surface.

In Table II, the simulated short-circuit current density (J_{SC}), the open-circuit voltage (V_{OC}), the fill factor (FF), the effective albedo (R_A), the maximum efficiency and maximum power output considering effective albedo, and spectral albedo are presented. We find again that white sand and snow show a high increase in short-circuit current density to 68.12 and

This article has been accepted for inclusion in a future issue of this journal. Content is final as presented, with the exception of pagination.

TABLE I
IDEAL BANDGAP, THERMODYNAMIC EFFICIENCY LIMIT, AND MAXIMUM POWER OUTPUT FOR DIFFERENT SPECTRAL AND EFFECTIVE ALBEDOS

	Optimal Bandgap (eV)	J_{SC} (Eff. Alb.) mA/cm^2	J_{SC} (Spec. Alb.) mA/cm^2	V_{OC} (Eff. Alb.) mV	V_{OC} (Spec. Alb.) mV	FF %	R_A	Efficiency (Eff. Alb.) %	Efficiency (Spec. Alb.) %	Power output (Eff. Alb.) W/m^2	Power output (Spec. Alb.) W/m^2
AM1.5 G	1.34	35.18	35.18	1060.1	1060.1	89	0	33.08	33.08	330.96	330.96
Green Grass	1.13	54.08	55.51	871.9	872.6	87	0.24	33.27	33.83	409.88	421.06
White Sand	1.34	58.73	61.03	1073.4	1074.4	89	0.67	33.53	34.88	560.44	582.59
Red Brick	1.13	53.84	52.35	871.8	871.1	87	0.24	33.27	31.99	407.97	396.29
Roofing Shingle	1.34	44.31	44.75	1066.1	1066.3	89	0.26	33.28	33.62	415.23	423.70
Dry Grass	1.13	62.48	62.93	875.6	875.9	87	0.44	33.40	33.38	475.77	479.92
Construction Concrete	1.34	45.28	44.84	1066.6	1066.4	89	0.29	33.30	32.98	428.78	424.57
Snow	1.34	65.00	69.25	1076.0	1077.6	89	0.85	33.62	35.88	616.88	663.17
AM1.5 G + Back Reflector	1.34	35.18	35.18	1078.0	1078.0	89	0	33.69	33.69	337.06	337.06

TABLE II
THERMODYNAMIC EFFICIENCY LIMIT AND MAXIMUM POWER OUTPUT FOR SILICON BIFACIAL SOLAR CELL UNDER DIFFERENT SPECTRAL ALBEDOS

	J_{SC} (Eff. Alb.) mA/cm^2	J_{SC} (Spec. Alb.) mA/cm^2	V_{OC} (Eff. Alb.) mV	V_{OC} (Spec. Alb.) mV	FF %	R_A	Efficiency (Eff. Alb.) %	Efficiency (Spec. Alb.) %	Power output (Eff. Alb.) W/m^2	Power output (Spec. Alb.) W/m^2
AM1.5 G	38.83	38.83	731.7	731.7	85	0	24.17	24.17	241.78	241.78
Green Grass	48.31	49.75	737.4	738.0	85	0.24	24.38	25.13	303.41	312.75
White Sand	64.82	68.12	745.0	746.1	85	0.67	24.67	25.96	411.95	433.53
Red Brick	48.09	46.83	737.3	736.5	85	0.24	24.37	23.72	301.90	293.80
Roofing Shingle	48.91	49.63	737.7	738.0	85	0.26	24.39	24.76	307.35	311.98
Dry Grass	55.80	56.59	741.1	741.3	85	0.44	24.52	24.87	352.48	357.53
Construction Concrete	49.98	50.12	738.2	738.2	85	0.29	24.41	24.48	314.28	315.16
Snow	71.74	75.58	747.6	748.9	85	0.85	24.76	26.14	457.71	483.07
Ideal Albedo	70.06	77.76	747.0	749.6	85	0.82	24.43	27.53	440.90	496.94

75.58 mA/cm^2, respectively, compared to 38.83 mA/cm^2 for AM 1.5G 1-sun illumination. The increased short-circuit current density together with an increase in open-circuit voltage leads to an efficiency of 25.96% and 26.14% for white sand and snow, respectively. These efficiencies are an absolute 1.29% and an absolute 1.38% higher than the expected efficiency if only taking a spectrally independent albedo into account. Only red brick yields a lower efficiency than expected from the effective albedo. For green grass and white sand, the power output is increased by 3.1% and 5.2%, respectively, when considering a spectrally dependent albedo. The power output is decreased by 2.7% for red brick, for a silicon bifacial solar cell. Note, in order to accurately determine the power output in a real solar cell, the power loss due to series resistance which scales with the square of the current at maximum power point needs to be taken into account.

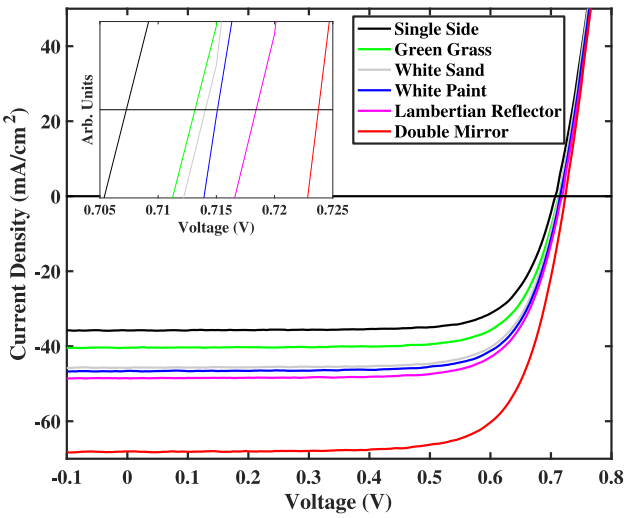

Fig. 4. Current–voltage characteristics of a bifacial solar cell under different illumination conditions.

V. EXPERIMENTAL STUDY

Bifacial silicon heterojunction (SHJ) solar cells were prepared on commercial grade <100> n-type CZ wafers with 3–5 Ω·cm resistivity and thickness of 180 μm. The alkaline texturing was followed by wet chemical cleaning and conditioning. The heterojunction was formed using plasma-enhanced chemical vapor deposition to grow intrinsic and doped hydrogenated amorphous layers (5–10 nm), forming a pi/CZ/in stack. ITO and silver contacts were sputtered on both sides of the wafer. The cell area of the devices amounts to 2 cm × 2 cm. The samples were annealed at 200 °C for 45 min. To experimentally characterize the performance of bifacial solar cells under various spectral albedos, a double illumination setup was used [32], [33]. In this setup, the solar cell is mounted under a 90°

This article has been accepted for inclusion in a future issue of this journal. Content is final as presented, with the exception of pagination.

TABLE III
OVERVIEW OF THE MEASURED PERFORMANCE OF THE BIFACIAL SOLAR CELL UNDER VARIOUS SPECTRAL ALBEDO CONDITIONS

	J_{SC} (Eff. Alb.) mA/cm^2	J_{SC} (Spec. Alb.) mA/cm^2	V_{OC} (Eff. Alb.) mV	V_{OC} (Spec. Alb.) mV	FF %	R_A	Efficiency (Eff. Alb.) %	Efficiency (Spec. Alb.) %	Power output (Eff. Alb.) W/m^2	Power output (Spec. Alb.) W/m^2	Power output Increase %
Single Side	35.8 ± 0.01	35.8 ± 0.01	707.3 ± 0.20	707.3 ± 0.20	74.9 ± 0.05	0	18.97 ± 0.03	18.97 ± 0.03	189.66 ± 0.3	189.66 ± 0.3	0
Double Mirror	68.1 ± 0.01	68.1 ± 0.01	723.8 ± 0.20	723.8 ± 0.20	73.8 ± 0.05	1	18.19 ± 0.02	18.19 ± 0.02	363.77 ± 0.4	363.77 ± 0.4	0
Green Grass	40.2 ± 0.02	40.4 ± 0.01	710.3 ± 0.20	713.2 ± 0.20	74.8 ± 0.05	0.12	19.07 ± 0.03	19.24 ± 0.03	213.58 ± 0.3	215.53 ± 0.3	0.91 ± 0.01
White Sand	45.1 ± 0.01	45.8 ± 0.01	713.3 ± 0.30	714.1 ± 0.20	74.3 ± 0.05	0.26	18.97 ± 0.03	19.29 ± 0.02	239.02 ± 0.3	243.00 ± 0.3	1.67 ± 0.01
White Paint	46.9 ± 0.01	46.6 ± 0.01	714.3 ± 0.20	715.1 ± 0.20	74.3 ± 0.05	0.31	19.01 ± 0.02	18.90 ± 0.02	249.07 ± 0.3	247.60 ± 0.3	-0.59 ± 0.01
Lambertian Reflector	48.88 ± 0.01	48.5 ± 0.01	715.4 ± 0.30	718.4 ± 0.20	74.3 ± 0.05	0.37	18.96 ± 0.03	18.90 ± 0.02	259.82 ± 0.3	258.88 ± 0.3	-0.36 ± 0.01

angle to the light source. Protected silver mirrors (Thorlabs PFSQ20-03-P01) were arranged under a 45° angle to the light source to simultaneously illuminate the bifacial solar cell from both sides at normal incidence without inducing self-shading. Current–voltage (*I–V*) measurements were performed with a xenon lamp and an AM 1.5G filter. The setup was calibrated with a reference cell of similar cell area to obtain 1-sun AM 1.5G illumination from both mirrors. The bifacial cell was then characterized under illumination from both mirrors (2 sun) and a single mirror (1 sun). Afterwards, one of the mirrors was replaced by different surfaces: green grass, white sand, white paint (white flat latex paint), and nearly ideal Lambertian unity reflectance paint ($BaSO_4$, 6080 white reflectance coating; LabSphere). A thermocouple was thermally connected to the solar cell to ensure constant temperature for all measurements. Fig. 4 shows the *I–V* characteristics under the above-described different conditions. The black curve in Fig. 4 shows the *I–V* characteristics for 1-sun AM 1.5G illumination via a single mirror on one side of the bifacial solar cell; the red curve presents double illumination with two mirrors. The green curve shows the *I–V* characteristics with green grass, grey stands for white sand, blue for white paint, and purple for the Lambertian reflector. By varying the incoming illumination spectrum on the rear side of the bifacial solar cell, J_{SC} is increased depending on the type of reflecting ground surface. Due to the logarithmic behavior of the voltage, depending on J_{SC}, a corresponding increase in V_{OC} is observed as predicted by theory (1). The increase in V_{OC} becomes clear from the inset in Fig. 4.

The double mirror configuration leads to the highest increase in J_{SC}. J_{SC} is almost doubled; the difference arises from high series resistance seen by the decreased fill factor. This trend of decreasing fill factor with increasing J_{SC} is visible for all the different surfaces due to the increase in series resistance as shown in Table III. In order to compare these results with our theoretical findings, we measured the spectral albedo of our different surfaces. A chopped, monochromated light source was used to illuminate the respective surface, and the photocurrent density of the bifacial solar cell was measured with a lock-in amplifier. Furthermore, the photocurrent that is generated with direct illumination by the monochromated light is measured. The spectral albedo is obtained from the ratio of these two measurements. Furthermore, we normalized the spectra to reflect the J_{SC} increase, taking the measured EQE of the bifacial solar cell into account. This step is necessary due to the diffuse reflection properties of the reflective surfaces. Fig. 5 shows the normalized measured spectral albedo data of the four surfaces used in our experiment.

In particular from the spectrum of the green grass, it can be seen that our measurement is very close to the Jet Propulsion Laboratory reference albedo data. In order to calculate the effective albedo (which is defined over the whole solar spectrum), we extended our measured spectra using the data of the Jet Propulsion Laboratory. For white paint and the Lambertian reflector surfaces, no literature reference data were available, so for these two surfaces, the spectrum was not extended over the whole solar spectrum to calculate the effective albedo. Table III presents an overview of the measurement results and the calculated effective albedos as well as J_{SC}, V_{OC}, efficiency, and power output, one would calculate from the effective albedo [using (1) and (4)]. Systematic errors of the measurement setup and errors due to temperature fluctuations are included to Table III. The change in fill factor is assumed to be negligible when taking effective albedo into account, and for this reason, the measured fill factor is used to determine the efficiency and power output. However, the series resistance increases with the square of the current at maximum power point, and therefore increases when accepting additional photons if the metal grid is not adapted. This leads to decrease in fill factor as can be seen from the measurements with single and double side illumination. The increase in power output is 0.91% for green grass and 1.67% for white sand. The increase is lower than expected from the calculations (see Table II) which is due to lower intensity of the reflected light. The overall experimental intensity was approximately a third of what was assumed in the calculations. The calculations assumed exposure of an infinite-area reflective albedo surface while the reflecting albedo surface and the illumination spot size were limited in our experiment. However, the ratio of the increase of power output when using green grass and white sand is identical between theory and experiment. The power output increase for white paint and the Lambertian reflector is negative and close to zero. This is expected from the nearly wavelength-independent spectral albedos for these materials (see Fig. 5). In fact, the deviation between effective and spectral albedo is the smallest for the Lambertian reflector validating our assumption that this surface has a reflectance very close to an ideal Lambertian reflector.

This article has been accepted for inclusion in a future issue of this journal. Content is final as presented, with the exception of pagination.

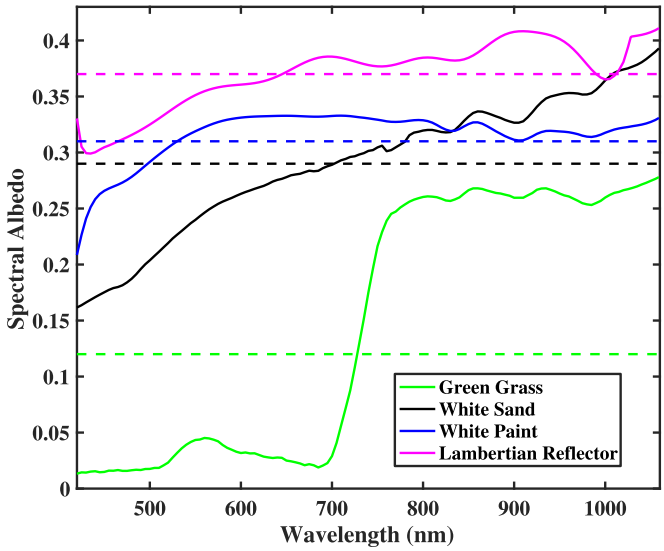

Fig. 5. Measured spectral albedo for the various reflecting surfaces.

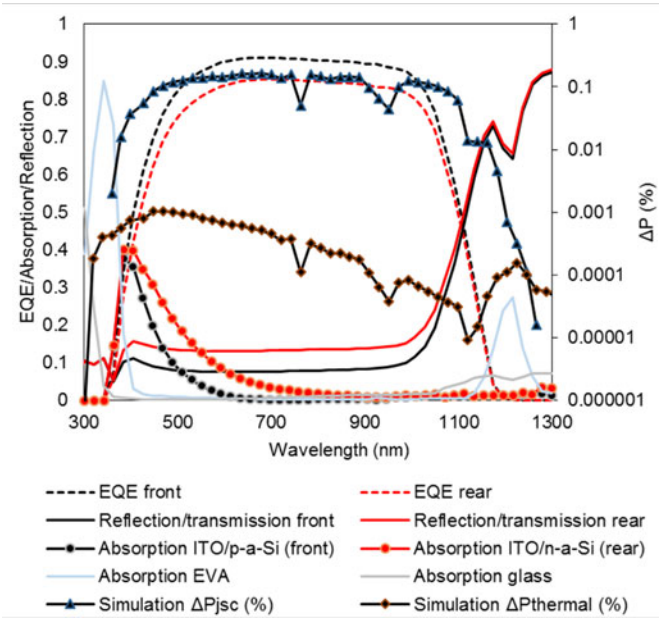

Fig. 6. Computationally simulated EQE, parasitic absorption, reflection, and transmission of a bifacial silicon heterojunction solar cell and the wavelength-dependent power gain and loss.

VI. Ideal Spectral Albedo

Our study raises the question about the existence of an ideal spectral albedo. Ultimately, this question is answered by calculating whether an incoming photon adds to the power output by increasing the current density or whether it has negative impact by increasing the temperature. For small assumed perturbations in the incident flux (i.e., no change in V_{OC}), the power output increase due to extra photons is described by

$$\Delta P_{j_{\mathrm{sc}}}(\lambda) \approx \frac{P_0}{j_{\mathrm{sc}_0}}\left(j_{\mathrm{sc}_0} + \Delta j_{\mathrm{sc}}\left(\mathrm{EQE}(\lambda)\right)\right). \tag{8}$$

With P_0 and j_{sc_0} being the power output and short-circuit current density, respectively, before adding photons by reflection of the surroundings. The additional short-circuit density (Δj_{sc}) that is generated by reflected photons depends on the EQE of the solar cell at the particular wavelength (λ). The decrease in power output due to heating of the solar cell is given by

$$\Delta P_{\mathrm{th}}(\lambda) = \Delta P\left(\Delta T(\lambda)\right). \tag{9}$$

With $\Delta P(\Delta T)$ being the temperature-dependent power output of the solar cell for a temperature increase of ΔT. The increase in temperature arises from (1) photons with energy $E_{\mathrm{ph}}(\lambda)$ that are parasitically absorbed $(A(\lambda))$ in nonactive layers and do not contribute to the current and (2) thermalization losses of photons with energy above band gap (E_{gap}). ΔT can be calculated from

$$\Delta T(\lambda) = \frac{\left(E_{\mathrm{ph}}(\lambda) - E_{\mathrm{gap}}\right)\cdot \mathrm{EQE}(\lambda) + E_{\mathrm{ph}}(\lambda)\cdot A(\lambda)}{c_p} \tag{10}$$

where c_p is the specific heat capacity of the absorber material. Note, that this expression neglects heat exchange with the environment due to radiation or convection, and therefore constitutes an upper boundary for the temperature. The lower boundary would be no change in temperature. At realistic conditions, the temperature strongly depends on the environmental conditions such as ambient temperature and wind speed [34]. As can be seen below, both boundaries lead to the same ideal spectral albedo.

An ideal material reflects all photons that are beneficial for the cell power output but does not reflect any photons that are detrimental. Therefore, the ideal spectral albedo is

$$R_A(\lambda) = \begin{cases} 1 \text{ if } |\Delta P_{j_{\mathrm{sc}}}(\lambda)| > |\Delta P_{\mathrm{th}}(\lambda)| \\ 0 \text{ if } |\Delta P_{j_{\mathrm{sc}}}(\lambda)| < |\Delta P_{\mathrm{th}}(\lambda)| \end{cases}. \tag{11}$$

The ideal spectral albedo for a silicon photovoltaic module is shown in Fig. 1, the effective albedo was calculated from the spectral albedo using (3). The calculation was performed taking the thermal power output decrease of a Panasonic HIT double 225 module.

For the calculation, a wavelength-dependent photon density equivalent to the AM 1.5G solar spectrum was assumed. It can be seen that the absorption of additional photons is beneficial as long as the EQE exceeds 0.1% in this case for all photons with wavelength <1250 nm.

The EQE and parasitic absorption were extracted from the literature [35]–[38] as well as from a computational simulation of a realistic SHJ module. The module consists of 180 μm crystalline silicon absorber, p-doped a-Si and 6% metal contact coverage on the front side, and n-doped a-Si and 12% metal contact coverage at the rear side. Furthermore, 450 μm EVA [39] and 3.2 mm glass [40] with antireflection coating [41] were assumed. Heat capacity and density of silicon were obtained from [42]. Fig. 6 presents the simulated EQE, parasitic absorption, reflection, and transmission of a bifacial SHJ solar cell and the wavelength-dependent power gain and loss. The power output for the ideal spectral albedo for a silicon bifacial solar cell is 496.94 W/m^2 (see Table II).

This article has been accepted for inclusion in a future issue of this journal. Content is final as presented, with the exception of pagination.

VII. Conclusion

We show that the spectral albedo significantly affects the thermodynamic efficiency limits and can considerably alter the resulting power output. The spectral albedo of snow, white sand, or green grass leads to a higher than expected power output relative to the effective albedo while red brick and construction concrete exhibit lower efficiencies. In the case of snow and white sand, the power outputs are increased by 7.5% and by 4.0%, respectively, when taking a spectrally dependent albedo into account. However, for red brick, the power output is 2.9% lower than predicted when only taking the effective albedo into account. For universal modeling of the power output boost in a real bifacial solar power plant, the location, weather condition, geometrical factors, and self-shading have to be taken into account. We show that the spectral albedo is a further important factor that should be used as input for these location-specific universal studies [43]–[46]. Furthermore, we derived the ideal spectral albedo for maximum power output and minimum heat impact which demonstrates opportunities for the development of artificial ground surfaces.

Acknowledgment

The authors would like to thank P. Jahelka and S. Yalamanchili.

References

[1] R. Kopecek *et al.*, "Bifaciality: One small step for technology, one giant leap for kWh cost reduction," *Photovolt. Int.*, vol. 26, pp. 32–45, 2014.
[2] F. Fertig *et al.*, "Economic feasibility of bifacial silicon solar cells," *Prog. Photovolt. Res. Appl.*, vol. 24, pp. 800–817, 2016.
[3] M. Hiroshi, "Radiation energy transducing device," US Patent 3278811 A, Oct. 11, 1966.
[4] A. Cuevas, A. Luque, J. Eguren, and J. Del Alamo, "50 Per cent more output power from an albedo-collecting flat panel using bifacial solar cells," *Sol. Energy*, vol. 29, pp. 419–420, 1982.
[5] C. E. Valdivia *et al.*, "Bifacial photovoltaic module energy yield calculation and analysis," in *Proc. 2017 IEEE Photovolt. Spec. Conf.*, 2017, to be published.
[6] B. Soria, E. Gerritsen, P. Lefillastre, and J. E. Broquin, "A study of the annual performance of bifacial photovoltaic modules in the case of vertical facade integration," *Energy Sci. Eng.*, vol. 4, pp. 52–68, 2016.
[7] L. Kreinin, A. Karsenty, D. Grobgeld, and N. Eisenberg, "PV systems based on bifacial modules: Performance simulation vs. design factors," in *Proc. 2016 IEEE 43rd Photovolt. Spec. Conf.*, 2016, pp. 2688–2691.
[8] C. Deline *et al.*, "Evaluation and field assessment of bifacial photovoltaic module power rating methodologies," in *Proc. 2016 IEEE 43rd Photovolt. Spec. Conf.*, 2016, pp. 3698–3703.
[9] C. W. Hansen *et al.*, "Analysis of irradiance models for bifacial PV modules," in *Proc. 2016 IEEE 43rd Photovolt. Spec. Conf.*, 2016, pp. 0138–0143.
[10] U. A. Yusufoglu *et al.*, "Analysis of the annual performance of bifacial modules and optimization methods," *IEEE J. Photovolt.*, vol. 5, no. 1, pp. 320–328, Jan. 2015.
[11] C. K. Lo, Y. S. Lim, and F. A. Rahman, "New integrated simulation tool for the optimum design of bifacial solar panel with reflectors on a specific site," *Renewable Energy*, vol. 81, pp. 293–307, 2015.
[12] A. Krenzinger and E. Lorenzo, "Estimation of radiation incident on bifacial albedo-collecting panels," *Int. J. Sol. Energy*, vol. 4, pp. 297–319, 1986.
[13] S. Guo, T. M. Walsh, and M. Peters, "Vertically mounted bifacial photovoltaic modules: A global analysis," *Energy*, vol. 61, pp. 447–454, 2013.
[14] M. Brennan, A. Abramase, R. W. Andrews, and J. M. Pearce, "Effects of spectral albedo on solar photovoltaic devices," *Sol. Energy Mater. Sol. Cells*, vol. 124, pp. 111–116, 2014.
[15] R. W. Andrews and J. M. Pearce, "The effect of spectral albedo on amorphous silicon and crystalline silicon solar photovoltaic device performance," *Sol. Energy*, vol. 91, pp. 233–241, 2013.
[16] W. Shockley and H. J. Queisser, "Detailed balance limit of efficiency of p-n junction solar cells," *J. Appl. Phys.*, vol. 32, pp. 510–519, 1961.
[17] ISE Fraunhofer, "Photovoltaics report," Fraunhofer ISE, Freiburg, Germany, 2014.
[18] F. Fertig *et al.*, "Bifacial potential of single-and double-sided collecting silicon solar cells," *Prog. Photovolt. Res. Appl.*, vol. 24, pp. 818–829, 2016.
[19] L. C. Hirst and N. J. Ekins-Daukes, "Fundamental losses in solar cells," *Prog. Photovolt. Res. Appl.*, vol. 19, pp. 286–293, 2011.
[20] M. R. Khan and M. A. Alam, "Thermodynamic limit of bifacial double-junction tandem solar cells," *Appl. Phys. Lett.*, vol. 107, 2015, Art. no. 223502.
[21] M. A. Green, "The path to 25% silicon solar cell efficiency: history of silicon cell evolution," *Prog. Photovolt. Res. Appl.*, vol. 17, pp. 183–189, 2009.
[22] A. Baldridge, S. Hook, C. Grove, and G. Rivera, "The ASTER spectral library version 2.0," *Remote Sens. Environ.*, vol. 113, pp. 711–715, 2009.
[23] M. A. Green, "Self-consistent optical parameters of intrinsic silicon at 300K including temperature coefficients," *Sol. Energy Mater. Sol. Cells*, vol. 92, pp. 1305–1310, 2008.
[24] Z. C. Holman *et al.*, "Infrared light management in high-efficiency silicon heterojunction and rear-passivated solar cells," *J. Appl. Phys.*, vol. 113, 2013, Art. no. 013107.
[25] Y. Han, X. Yu, D. Wang, and D. Yang, "Formation of various pyramidal structures on monocrystalline silicon surface and their influence on the solar cells," *J. Nanomater.*, vol. 2013, 2013, Art. no. 716012.
[26] E. Yablonovitch, "Photonic crystals: Semiconductors of light," *Sci. Amer.*, vol. 285, pp. 46–55, 2001.
[27] M. A. Green, "Radiative efficiency of state-of-the-art photovoltaic cells," *Prog. Photovolt. Res. Appl.*, vol. 20, pp. 472–476, 2012.
[28] K. R. McIntosh and S. C. Baker-Finch, "OPAL 2: Rapid optical simulation of silicon solar cells," in *Proc. 2012 38th IEEE Photovolt. Spec. Conf.*, 2012, pp. 000265–000271.
[29] R. Saive *et al.*, "Effectively transparent front contacts for optoelectronic devices," *Adv. Opt. Mater.*, vol. 4, pp. 1470–1474, 2016.
[30] R. Saive *et al.*, "Effectively transparent contacts (ETCs) for solar cells," in *Proc. 2016 IEEE 43rd Photovolt. Spec. Conf.*, 2016, pp. 3612–3615.
[31] R. Saive *et al.*, "Silicon heterojunction solar cells with effectively transparent front contacts," *Sustain. Energy Fuels*, vol. 1, pp. 593–598, 2017.
[32] M. Ezquer, I. Petrina, J. Cuadra, A. Lagunas, and F. Cener-Ciemat, "Design of a special set-up for the IV characterization of bifacial photovoltaic solar cells," in *Proc. 24th Eur. Photovolt. Sol. Energy Conf. Exhib.*, Hamburg, Germany, 2009, pp. 1553–1556.
[33] H. Ohtsuka *et al.*, "Characteristics of bifacial solar cells under bifacial illumination with various intensity levels," *Prog. Photovolt. Res. Appl.*, vol. 9, pp. 1–13, 2001.
[34] C. Schwingshackl *et al.*, "Wind effect on PV module temperature: Analysis of different techniques for an accurate estimation," *Energy Procedia*, vol. 40, pp. 77–86, 2013.
[35] M. A. Green *et al.*, "Solar cell efficiency tables (version 49)," *Prog. Photovolt. Res. Appl.*, vol. 25, pp. 3–13, 2017.
[36] L. Yang *et al.*, "High efficiency screen printed bifacial solar cells on monocrystalline CZ silicon," *Prog. Photovolt. Res. Appl.*, vol. 19, pp. 275–279, 2011.
[37] T. Dullweber *et al.*, "The PERC+ cell: A 21%-efficient industrial bifacial PERC solar cell," in *Proc. 31st Eur. Photovolt. Sol. Energy Conf. Exhib.*, 2015, pp. 341–350.
[38] C. Duran, "Bifacial solar cells: High efficiency design, characterization, modules and applications," Doctoral dissertation, Univ. Konstanz, Konstanz, Germany, 2012.
[39] M. R. Vogt *et al.*, "Optical constants of UV transparent EVA and the impact on the PV module output power under realistic irradiation," *Energy Procedia*, vol. 92, pp. 523–530, 2016.
[40] M. R. Vogt *et al.*, "Measurement of the optical constants of soda-lime glasses in dependence of iron content and modeling of iron-related power losses in crystalline Si solar cell modules," *IEEE J. Photovolt.*, vol. 6, no. 1, pp. 111–118, Jan. 2016.
[41] M. R. Vogt, "Development of physical models for the simulation of optical properties of solar cell modules," Ph.D. dissertation, Technische Informationsbibliothek, Hanover, Germany, 2016.

This article has been accepted for inclusion in a future issue of this journal. Content is final as presented, with the exception of pagination.

[42] R. K. Endo, Y. Fujihara, and M. Susa, "Calculation of the density and heat capacity of silicon by molecular dynamics simulation," *High Temp. High Press.*, vol. 35, pp. 505–511, 2003.

[43] A. A. B. Baloch, M. Armoush, B. Hindi, A. Bousselham, and N. Tabet, "Performance assessment of stand alone bifacial solar panel under real time conditions," in *Proc. 2017 IEEE Photovolt. Spec. Conf.*, 2017, to be published.

[44] L. Kreinin *et al.*, "PV module power gain due to bifacial design. Preliminary experimental and simulation data," in *Proc. 2010 35th IEEE Photovolt. Spec. Conf.*, 2010, pp. 002171–002175.

[45] U. A. Yusufoglu *et al.*, "Simulation of energy production by bifacial modules with revision of ground reflection," *Energy Procedia*, vol. 55, pp. 389–395, 2014.

[46] X. Sun, M. R. H. Khan, Amir, M. M. Hussain, and M. A. Alam, "The potential of bifacial photovoltaics: A global perspective," in *Proc. 2017 IEEE Photovolt. Spec. Conf.*, 2017, to be published.

Authors' photographs and biographies not available at the time of publication.